Synthesis and properties of the vacancy-free $La_{1-x}Ba_xMnO_3$

B. Dabrowski, K. Rogacki,* X. Xiong, P. W. Klamut,* R. Dybzinski, and J. Shaffer
Department of Physics, Northern Illinois University, DeKalb, Illinois 60115

J. D. Jorgensen
Materials Science Division, Argonne National Laboratory, Argonne, Illinois 60439
(Received 4 February 1998)

Thermogravimetric analysis was used to determine the synthesis conditions for obtaining samples of the Ba-substituted $LaMnO_3$ with stoichiometric oxygen content. Single-phase and vacancy-free samples of $La_{1-x}Ba_xMnO_3$ have been prepared for $x=0.12-0.24$ in air by quenching from 1100–1450 °C. The $x<0.12$ compositions require synthesis under reduced oxygen pressure. The structure was studied using neutron powder diffraction and is discussed in the framework of the tolerance factor concept. At room temperature, the structural transition from orthorhombic to rhombohedral symmetry occurs around $x=0.13$. The structural, magnetic, and resistive measurements show that properties are similar to the Sr-substituted system for slightly smaller substitution level. Curie temperatures are higher than for the Sr-substituted samples for small x, $x=0.10-0.14$, due to a better match of the Mn-O and La(Ba)-O bond lengths, and are slightly lower for larger x, $x=0.20-0.24$ due to an increased local distortion. The largest magnetoresistive effect at room temperature was found for $x=0.22$. By comparing the Ba- and Sr-substituted systems it is shown that structural properties are governed by the ionic sizes while physical properties are controlled by both the ionic sizes and the hole doping. [S0163-1829(98)01529-X]

INTRODUCTION

Pure and substituted $LaMnO_3$ materials are of considerable current interest owing to a colossal decrease of resistivity in the applied magnetic field near the Curie temperature that can be controlled by the hole doping and the sizes of the substituted alkaline and rare-earth ions.[1] Research on pure $LaMnO_3$ has shown that large deviations from nominal stoichiometry can be caused by the formation of vacancies on the metal sites while the oxygen network is believed to remain vacancy free leading to compositions normally written as $LaMnO_{3+\delta}(\delta>0)$.[2–5] The perovskite structure of $LaMnO_3$ can accommodate large concentrations of vacancies on both the A (La/Ba) and B (Mn) sites as a result of synthesis under oxidizing conditions.[2–4] The vacancy concentrations are asserted to be the same on both the A and B sites.[4,5] Formation of the vacancies increases the average Mn oxidation state above 3+ and causes large local distortions.[3] The work on the alkaline-earth-substituted materials indicates that vacant metal sites are still present even at the moderate substitution levels, $x\sim0.15$.[4] To date a detailed knowledge of the vacancy concentrations as a function of substitution level, synthesis temperature, and oxygen partial pressure is absent.

Most of the recent publications on both powders and single crystals of the Ca, Sr, and Ba-substituted $LaMnO_3$ materials do not specify the vacancy concentrations of the samples. However, such defects are likely to exist because the synthesis conditions range from annealings in 200 atm of oxygen at 650 °C to annealings in air or argon at 1500 °C and higher temperatures.[5–10] This could explain significant differences in behavior when it was assumed that measurements were made on equivalent samples. For example, work on $La_{0.83}Sr_{0.17}MnO_3$ single crystals annealed under several temperatures and oxygen pressures indicates large variations of the magnetic and transport properties as a function of the annealing conditions that govern the defect concentration.[11] Since the vacant metal sites dope holes much more effectively than alkaline-earth substitutions, and the phase diagrams are complex and very sensitive to the hole concentration, it is of critical importance to establish the Mn oxidation level, i.e., to establish both the cation substitution level x and the vacancy concentration v.

We report here on a study of the synthesis, vacancy concentration, structure, and physical properties of vacancy-free, $v\sim0$, Ba-substituted material. To date, a limited amount of work on these compositions has been done and no reliable data are available for the properties as a function of hole doping.[6] Using thermogravimetric analysis we have determined the synthesis conditions and have prepared vacancy-free samples for $x=0.10-0.24$. The structural and physical properties of the single-phase vacancy-free samples are reported here and compared with those for Sr- and Ca-substituted materials.

EXPERIMENTAL

Polycrystalline samples of $La_{1-x}Ba_xMnO_3$ ($x=0.10-0.24$) were synthesized from stoichiometric mixtures of La_2O_3 (prefired in Ar at 750 °C), MnO, and $BaCO_3$. Samples of about 10 g were fired in air at various temperatures up to 1450 °C followed by fast cooling to room temperature on a Cu plate. The samples were heated for several days with frequent intermediate grindings. The high-pressure annealings were done for several days in pure oxygen (120 atm O_2) at 800 °C. Sample homogeneity was checked by powder x-ray diffraction. The oxygen contents were determined by thermogravimetric analysis measurements using a Cahn TG

171 system with slow (0.6 deg/min) heating and cooling rates. Neutron powder-diffraction data were obtained using the Special Environment Powder Diffractometer at Argonne National Laboratory's Intense Pulsed Neutron Source. Magnetization, susceptibility, and magnetoresistance measurements were performed with a Quantum Design Physical Properties Measurement System.

SYNTHESIS AND DEFECTS

Our aim was to prepare vacancy-free $La_{1-x}Ba_xMnO_3$ samples with properties that would be a function of only the amount of the substituted ion. Of interest were compositions for which the structural, orthorhombic-to-rhombohedral, and magnetoresistive transitions would appear near room temperature. Samples with compositions $x=0.10-0.24$ were chosen for that reason. All samples, prepared in air at temperatures 1150–1450 °C, in argon at 1150 °C, or at high oxygen pressure (120 atm O_2) at 800 °C, were single phase according to x-ray diffraction. However, structural as well as physical properties were very sensitive to the synthesis temperature and the oxygen pressure. The properties of materials with various amounts of vacancies that were synthesized under several synthesis conditions, will be the subject of a separate publication.

To measure the oxygen content and determine the synthesis conditions for vacancy-free samples, high sensitivity thermogravimetric analysis (TGA) measurements were used. After synthesis in air at 1350 °C, the $x=0.12$, 0.16, 0.20, and 0.24 samples were annealed at 120 atm, O_2 at 800 °C for two days and fast cooled to room temperature. These samples were subjected to two consecutive TGA runs: First, slowly heated to 1400 °C and cooled to room temperature in 20% O_2/Ar gas mixture, and second, slowly heated to 1300 °C and fast cooled to room temperature in pure Ar ($\sim$10 ppm O_2). In an attempt to obtain a fixed point for the normalization of the oxygen content, an additional TGA run was done in 50% H_2/Ar to 1300 °C. X-ray diffraction of the reduced materials revealed the presence of three phases, La_2O_3, MnO, and layered $(La, Ba)_3Mn_2O_y$. Since the precise La/Ba ratio and the oxygen content of the layered phase are not known, we could not use the observed weight losses in hydrogen to establish the absolute oxygen content. Thus, the oxygen content was assigned to be 3.000 atoms per molecule of $La_{1-x}Ba_xMn$ at the center of the extended weight loss plateau in Ar observed near 1100 °C (see Fig. 1). An absolute oxygen content of 3.000 was confirmed at this plateau for $LaMnO_3$ from a reduction in hydrogen to La_2O_3 and MnO. Figure 1 shows the TGA data for the $x=0.16$ sample. The starting material annealed at high oxygen pressure has an effective oxygen content $3+\delta=3.092\pm0.002$. Since, according to the data for pure $LaMnO_3$,[3–5] there is no excess oxygen in the structure, but vacancies form in equal amounts on both metal sites A and B, we can estimate the vacancy concentration ($v\sim\delta/\delta+3$), $v\sim0.03$. This large defect concentration causes a significant increase of the doping level, $\Delta h=2\delta\sim6v\sim0.18$, and also introduces local structural distortions and electronic inhomogeneity that affect the magnetic and transport properties.

The data taken on heating and cooling in 20% O_2 are almost fully reproducible in the temperature range 1100–1400 °C ($\Delta\delta<0.002$); i.e., the sample is close to thermal equilibrium when heated/cooled at 0.6 deg/min. On heating, the oxygen content is very close to 3.000 around 1350 °C. The oxygen content at 1400 °C is slightly less than 3.000 and gradually decreases to 2.998 ± 0.002 over a period of 2 h at constant temperature. On cooling to 700 °C, the oxygen content increases to 3.018 ± 0.002. No significant changes in oxygen content are seen below 700 °C during either heating or cooling in 20% O_2. Also, heating in Ar does not change the oxygen content below 700 °C. On heating in argon at higher temperatures, between 700 and 1100 °C, the oxygen content gradually decreases to 3.000 ± 0.002 and than remains unchanged to 1200 °C. On continued heating, the oxygen content decreases to 2.997 ± 0.002 at 1300 °C and decreases further to 2.995 ± 0.002 during an additional hold at 1300 °C for 10 h. Thus, to make a vacancy-free $La_{0.84}Ba_{0.16}MnO_{3.000}$ sample an annealing in air at $\sim$1350 °C or in argon at $\sim$1100 °C should be used.

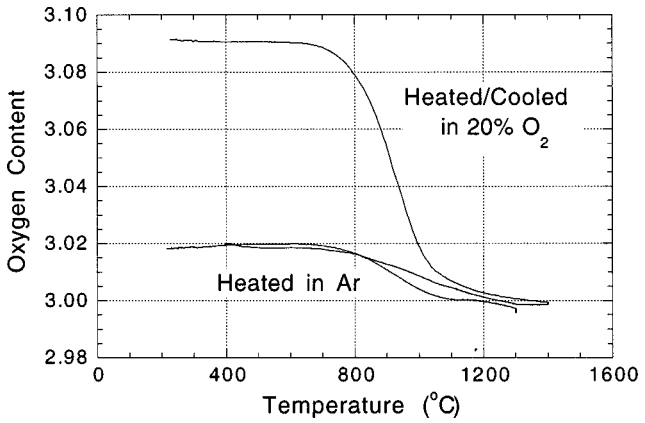

FIG. 1. Oxygen content determined by thermogravimetric analysis measurements in 20% O_2/Ar and Ar for the $La_{0.84}Ba_{0.16}MnO_y$ sample prepared in 120 atm O_2 at 800 °C.

While the magnetic properties of the samples with the same x prepared under these conditions are virtually identical, the resistive properties differ somewhat. The Ar-annealed sample shows higher resistivity. A slight decomposition of the material at the grain boundaries may cause the increased resistivity for the Ar-annealed sample. To obtain a consistent set of samples we have chosen to use synthesis in air as much as possible. Note also, that a constant oxygen content below 700 °C under various oxygen pressures suggests that the oxygen sublattice is fixed and the metal-site vacancies form only when metal atom diffusion is kinetically allowed above 700 °C. However, at very high temperatures in air, or above $\sim$1200 °C in argon, vacancies on the oxygen network can appear, possibly leading to the decomposition of the perovskite structure.

Figure 2 shows TGA data for several samples heated in 20% O_2 after the high-pressure oxygen anneal. The effective oxygen content after the high-pressure anneal is $3+\delta=3.128$, 3.055, and 3.032 (±0.002) for $x=0.12$, 0.20, and 0.24, respectively. The metal-site vacancies are thus $\sim$0.04, 0.02, and 0.01, respectively, corresponding again to a significant additional hole doping, $\Delta h\sim0.26$, 0.11, and 0.06, respectively. Clearly, the vacancy concentration that can be induced using high oxygen pressure annealing is very large and decreases with increased substitution level. The vacancy

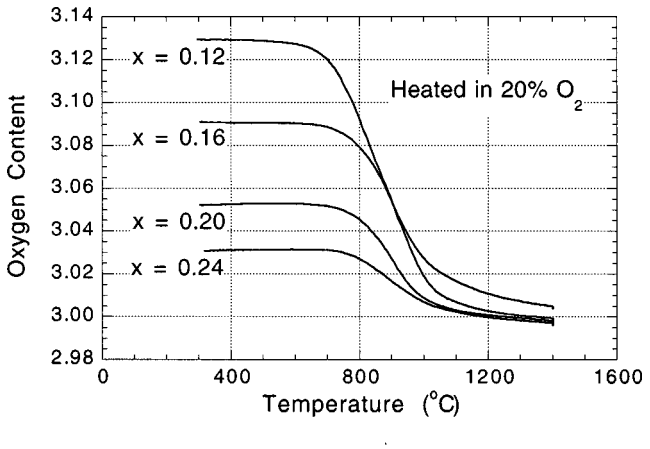

FIG. 2. Oxygen content determined by thermogravimetric analysis measurements on heating in 20% O_2/Ar for several $La_{1-x}Ba_xMnO_y$ samples prepared in 120 atm O_2 at 800 °C.

concentration that is obtained after a slow cooling in air (not shown) is smaller and depends also on the substitution level, $\delta = 0.040$, 0.005, and -0.002 (± 0.002) or $v \sim 0.013$, 0.002, and 0.000 for $x = 0.12$, 0.20, and 0.24, respectively.

Heating to 1400 °C and holding for 2 h in air was not sufficient to remove all metal-site vacancies for the $x = 0.12$ sample, $d = 0.003$ or $v \sim 0.001$, $\Delta h \sim 0.006$. To make that sample vacancy-free, we heated it in air at 1450 °C for 24 h. To make a vacancy-free sample with smaller $x = 0.10$ required even more reducing conditions of annealing in argon at 1100 °C. On the other hand, heating to 1400 °C and holding for 2 h in air makes the $x = 0.20$ and 0.24 samples deficient in oxygen, $\delta = -0.003$ and -0.004, respectively. However, the vacancy-free samples with these compositions, $x = 0.20$ and 0.24, can also be obtained in air at lower temperatures, ~1250 and 1150 °C, respectively. The synthesis conditions used for preparation of other, vacancy-free samples are given in Table I. It is worth noting that each composition requires unique synthesis conditions, therefore, a series of samples made under identical conditions will result in materials with varying vacancy content on the metal or oxygen sites. The TGA data presented here can be used to quantitatively measure the defect concentration induced under various synthesis conditions and may resolve inconsistencies reported in the literature.

STRUCTURAL CHARACTERIZATION

The powder neutron-diffraction data were collected for ~6 g samples at room temperature. Data were collected for $x = 0.10$, 0.12, 0.14, 0.16, 0.20, and 0.24 using all detectors banks, but only the higher resolution backscattering data ($\Delta d/d = 0.035$) were analyzed. Rietveld structural refinements were carried out using the GSAS code[12] over the d-spacing range $0.5 < d < 4.0$ Å. The background was modeled using an eight-term cosine Fourier series, and diffraction peaks were described using a two-sided exponential that was convoluted with a Gaussian and a Lorentian to describe the instrumental and sample contribution to the peak profile, respectively. For each pattern, atom positions and thermal parameters were refined. The observed and calculated patterns for the two samples with compositions $x = 0.10$ and 0.20 are shown in Figs. 3(a) and 3(b). Based on previous reports for Sr-substituted materials the patterns were indexed using an orthorhombic cell, space group $Pbnm$ for $x = 0.10$, and a rhombohedral cell, space group $R\text{-}3c$ for $x = 0.14$–0.24.[10] The $x = 0.12$ sample was two-phase, 97% orthorhombic and 3% rhombohedral, at room temperature. Thus, the structural orthorhombic-to-rhombohedral transition appears on Ba substitution around $x = 0.13$ at room temperature. The refined structural parameters and selected bond angles and distances are given in Table II.

Table II clearly shows that on Ba substitution the unit-cell volume and the Mn-O bond lengths decrease while the Mn-O-Mn bond angles increase toward 180°. A large Jahn-Teller distortion is present for the $x = 0.1$ sample but it is significantly decreased for $x = 0.12$, as is evidenced by the refined Mn-O bond lengths that converge to a similar value, and become equal for $x \geqslant 0.14$ in the rhombohedral phase. The observed changes of the unit-cell volume and the Mn-O bond lengths are consistent with a decreasing average Mn ionic size on oxidation from 3.1+ to 3.24+ caused by the increased hole doping. Both the Mn-O_a-Mn and Mn-O_e-Mn bond angles increase with increasing x as a result of the better match between the Mn-O and La(Ba)-O bond lengths; i.e., as a result of an increase of the tolerance factor, $t = [\langle R(A)\rangle + R(\mathrm{O})]/\sqrt{2}[\langle R(B)\rangle + R(\mathrm{O})]$, where $R(\mathrm{O}) = 1.40$ Å is the ionic size of the O^{2-} (for VI-coordinated radii) and $\langle R(A)\rangle$ and $\langle R(B)\rangle$ are the mean ionic sizes of ions on the A and B sites, respectively.[13] Decreasing Jahn-Teller distor-

TABLE I. Summary of synthesis conditions and structural, resistive, and magnetic properties for $La_{1-x}Ba_xMnO_3$.

x	0.10	0.12	0.14	0.16	0.18	0.20	0.22	0.24
Synthesis	Ar, 1100 °C	air, 1450 °C	air, 1400 °C	air, 1350 °C	air, 1300 °C	air, 1250 °C	air, 1200 °C	air, 1150 °C
(A-O)/$\sqrt{2}$(Mn-O)	0.989(1)	0.991(1)	0.990(1)	0.991(1)		0.993(1)		0.994(1)
$t(XII)$	0.968	0.971	0.974	0.977	0.980	0.983	0.986	0.988
$t(IX)$	0.918	0.921	0.924	0.927	0.930	0.933	0.935	0.938
T_M (K)	188	203	222	240	261	277	295	309
T_R (K)	185	198	222	243	263	282	296	310
T_c (K)	245		278		310		337	
μ_{eff}(exp) (μ_B)	4.82		4.86		4.74		4.66	
μ_{eff}(calc) (μ_B)	4.80		4.76		4.71		4.67	
μ_{sat}(exp) (μ_B)	3.93	3.92	3.92	3.88	3.89	3.88	3.84	3.81
μ_{sat}(calc) (μ_B)	3.90	3.88	3.86	3.84	3.82	3.80	3.78	3.76

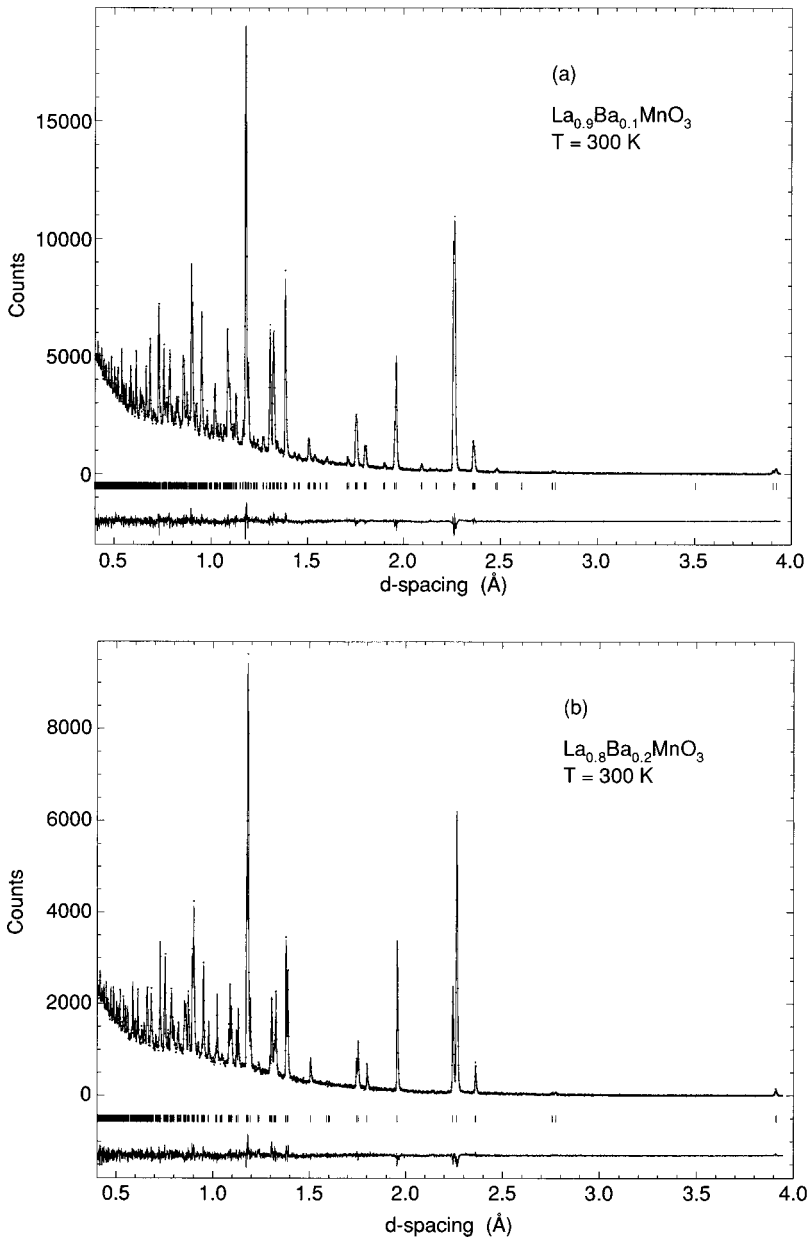

FIG. 3. Observed and calculated neutron-diffraction patterns for $La_{1-x}Ba_xMnO_{3.00}$ samples with compositions $x=0.10$ (a) and 0.20 (b).

tions were observed before at room temperature for Sr-substituted samples with compositions $x=0.1-0.17$ in the orthorhombic phase.[10,14] Bond lengths were equal for $x \geqslant 0.20$ in the rhombohedral phase.

At room temperature, the structural orthorhombic-to-rhombohedral transition occurs for the Ba-substituted material at a smaller substitution amount, $x\sim 0.13$, than for the Sr-substituted samples, $x\sim 0.165$.[7,8,14] For the Ba-substituted sample $x=0.14$ in the rhombohedral phase, the Mn-O-Mn bond angle and Mn-O bond length are 163.8(1)° and 1.977(2) Å, respectively. The value of the Mn-O-Mn bond angle is almost exactly the same as for the rhombohedral Sr-substituted sample with $x=0.175$, 163.60(6)°.[14] The similarity of the Mn-O-Mn bond angles at the orthorhombic-to-rhombohedral transition for the Ba- and Sr-substituted samples suggests that the structural transition is governed by the tolerance factor. Since the ionic size of Ba, $R(\mathrm{Ba})=1.61$ Å (for XII-coordinated ion), is considerably larger than that of Sr, $R(\mathrm{Sr})=1.44$ Å (for XII-coordinated ion), the tolerance factor increases faster with Ba substitution than with Sr substitution.[13] Thus, the materials with $x_{\mathrm{Ba}}=0.13$ and $x_{\mathrm{Sr}}=0.165$ have very similar tolerance factors, $t=0.975$ and 0.971, respectively. The Mn-O bond length for the Sr-substituted sample with $x=0.175$ is 1.968(2) Å, i.e., it is smaller than for the Ba-substituted sample with $x=0.14$ in agreement with the observation that the Mn-O bond lengths are controlled mostly by the hole doping level. The difference of the Mn-O bond lengths at the orthorhombic-to-rhombohedral transition for the Ba- and Sr-substituted samples suggests that the Mn-O bond lengths do not directly govern the structural transition but influence it indirectly through the tolerance factor.

A further difference between the Ba- and Sr-substituted samples results from the size differences among the La, Sr, and Ba ions. Since the ionic size of Ba is larger than Sr, the size difference between Ba and La [$R(\mathrm{La})=1.36$ Å for XII-

TABLE II. Summary of crystallographic data for $La_{1-x}Ba_xMnO_3$.

x	0.1	0.12	0.14	0.16	0.2	0.24
Space Group	*Pbnm*	*Pbnm*	*R*-3*c*	*R*-3*c*	*R*-3*c*	*R*-3*c*
a(Å)	5.5608(1)	5.5650(1)	5.5604(1)	5.5562(1)	5.5508(1)	5.5443(1)
b(Å)	5.5352(1)	5.5232(1)				
c(Å)	7.8150(1)	7.8148(1)	13.4497(2)	13.4510(1)	13.4649(2)	13.4809(3)
V	240.55(1)	240.20(1)	360.12(1)	359.62(1)	359.29(1)	358.87(2)
x_R[O(1)]			0.5502(1)	0.5484(1)	0.5435(1)	0.5376(2)
x[La/Ba]	−0.0038(3)	−0.0032(3)				
y[La/Ba]	0.4822(2)	0.4881(4)				
x[O(1)]	−0.0645(3)	−0.0631(3)				
y[O(1)]	−0.0053(4)	−0.0049(6)				
x[O(2)]	0.2331(3)	0.2369(4)				
y[O(2)]	0.2719(2)	0.2653(4)				
z[O(2)]	0.0342(1)	0.0329(2)				
U_{iso}(La/Ba)	0.58(6)	0.58(6)	0.52(7)	0.44(5)	0.53(6)	0.46(8)
U_{iso}(Mn)	0.43(9)	0.44(9)	0.5(1)	0.31(8)	0.35(9)	0.3(1)
U_{iso}(O1)	1.3(1)	1.2(1)	1.5(1)	1.44(5)	1.56(6)	1.43(7)
U_{iso}(O2)	1.3(1)	1.5(1)				
R_{wp}/χ^2	5.6/3.0	7.7/2.7	7.6/3.2	6.3/2.9	7.6/2.6	7.1/2.7
Mn-O(Å)			1.9775(1)	1.9752(1)	1.9710(1)	1.9665(1)
Mn-O-MN (°)			163.80(4)	164.36(4)	165.93(4)	167.83(5)
Mn-O_a (Å)	1.9864(3)	1.9853(4)				
Mn-O_{e1} (Å)	2.003(1)	1.987(2)				
Mn-O_{e2} (Å)	1.968(1)	1.973(2)				
Mn-O_a-Mn (°)	159.20(9)	159.5(1)				
Mn-O_e-Mn (°)	162.18(6)	163.69(8)				

coordinated ion] is considerably larger than between Sr and La. The local size variations of the *A*-site ion affect most profoundly the nearby oxygen ions. The effect of the local oxygen distortions is most visible in the isotropic thermal factors, U_{ISO}[O(1)]. The large refined isotropic thermal factors indicate that the oxygen atoms have considerable static displacements. Table II shows that the oxygen isotropic thermal factors are quite large but do not change significantly with x for the Ba-substituted samples. Comparison of the oxygen isotropic thermal factors to values measured for the Sr-substituted samples,[14] shows that the oxygen thermal factors are about 50% larger for Ba-substituted samples while the thermal factors for metal ions are quite similar. This observation supports the suggestion that the local oxygen distortions are larger for the Ba-substituted samples.

The convenience of using the tolerance factor to describe universal trends of structural and physical properties of substituted $LaMnO_3$ was recognized before.[9,15] However, most researchers used the IX-coordinated values of the ionic sizes to calculate tolerance factor. We argue that to properly calculate the tolerance factor and, thus, also the variance of the ionic radii one should use the XII-coordinated ionic radii for the perovskite structure.[13] Table I shows the calculated tolerance factors using IX- and XII-coordinated ionic radii and the measured ratio of the averaged (La/Ba-O)/$\sqrt{2}$(Mn-O) bond lengths. Clearly the measured values are much better described using the XII-coordinated ionic radii. Further evidence for using the XII-coordinated ionic radii comes from the observed solubility limits for the Sr ($x\sim0.6$) and Ba ($x\sim0.3$) substitutions which are close to compositions where the tolerance factor is 1 only when the XII-coordinated ionic sizes are used.

Rodrigues and Attfield[16] argued that the size differences between various *A*-site ions induce local distortions and stresses in the structure. The quantitative description of this effect was given in terms of the variance of the ionic radii $R(M)$, M=La, Sr, Ba, about the mean $\langle R(A)\rangle$, $s^2=\Sigma\{x_M R^2(M)-\langle R(A)\rangle^2\}$. To measure the Mn-O and La(M)-O bond length mismatches, Rodrigues and Attfield used the differences between the mean $\langle R(A)\rangle$ and the optimal *A*-site size, R_{opt} for the IX-coordinated *A*-site ions. The R_{opt} was defined as an *A*-site ion size for which the tolerance factor is equal to 1, i.e., $t=1=[R_{opt}+R(O)]/\sqrt{2}[\langle R(B)\rangle+R(O)]$. Figure 4 shows the calculated variance of the ionic radii s vs the difference between the optimal *A*-site size and mean, $r=R_{opt}-\langle R(A)\rangle$ for three series of substituted $LaMnO_3$ materials using the XII-coordinated *A*-site ions. The dots on the curves denote the increasing substitution level in intervals of 0.05 starting from pure $LaMnO_3$, $r=0.132$, and $s=0$ Å. The numbers near each curve are previously reported ferromagnetic transition temperatures[7,9,17] and our recent data for vacancy-free $La_{1-x}Sr_xMnO_3$ and $La_{1-x}Ca_xMnO_3$ samples.[14]

According to Rodrigues and Attfield the ferromagnetic transition temperatures are suppressed from the optimum, $T_c(\text{opt})\sim530$ K, because of the ordered and random local distortions generated, respectively, by the difference between the optimal *A*-site size and mean (r) and the variance of the ionic radii about the mean (s). The functional relation was

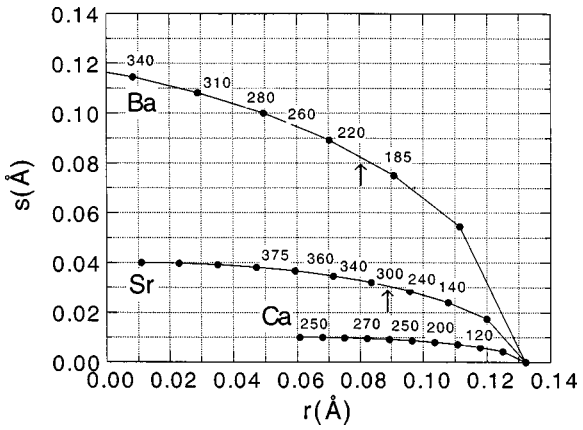

FIG. 4. Calculated variance of the ionic radii s vs the difference between the optimal and mean A- site size r for Ba-, Sr-, and Ca-substituted $LaMnO_3$ materials (see text). The dots on the curves denote the increasing substitution level in intervals of 0.05. The numbers near each curve are ferromagnetic transition temperatures.

found $T_c(s,r)=T_c(\text{opt})-p_1s^2-p_2r^2$ ($p_1=20\,600$ and $p_2=29\,000$ K/Å^2) for the $RR'_{0.7}MM'_{0.3}MnO_3$ samples with fixed substitution level and a constant mean A-site size ($\langle R(A)\rangle=1.23$ Å for the IX-coordinated A-site ions).[16] The data shown in Fig. 4 confirm that T_c decreases with increasing s and r. However it is not clear if T_c satisfies the functional form proposed by Rodrigues and Attfield. Moreover, T_c clearly depends also on the doping level h, as is evidenced for the $La_{1-x}Ca_xMnO_3$ system which shows almost constant and lower than expected values of T_c for $x=0.3-0.5$.

The arrows on Fig. 4 mark the compositions at which the structural, orthorhombic-to-rhombohedral, transition appear at room temperature for the Ba- and Sr-substituted samples. The data indicate that the Ca-substituted samples should show the orthorhombic-to-rhombohedral transition around $x=0.3$. However, all Ca-substituted compositions display the orthorhombic structure at room temperature for $x=0.2-0.5$.[17] In addition, the Ca-substituted samples show extremely sharp resistive transitions for $x=0.2-0.3$ and transitions of an unusual shape for $x=0.3-0.5$.[14] Comparison of the structural, magnetic, and resistive properties for the Ba- and Sr-substituted samples indicates somewhat singular behavior of the Ca-substituted samples with $x=0.3-0.5$.

MAGNETIC AND RESISTIVE PROPERTIES

To study the magnetic properties, the magnetization M was measured from 5 to 390 K in a dc applied field of 0.002–7 T. Measurements were performed as a function of temperature at a constant magnetic field for both the zero-field-cooled and field-cooled samples, and as a function of magnetic field at 6 K. The magnetizations at temperatures close to the magnetic transition in an applied field of 2 mT are shown in Fig. 5(a) for all samples, $x=0.10-0.24$ (in steps of $\Delta x=0.02$). Transitions from the paramagnetic to the ferromagnetic state are continuous and sharp for $x=0.14-0.22$, indicating good sample quality with a homogeneous distribution of substituted ions. Transitions for samples with $x=0.10$ and 0.12 are less regular suggesting

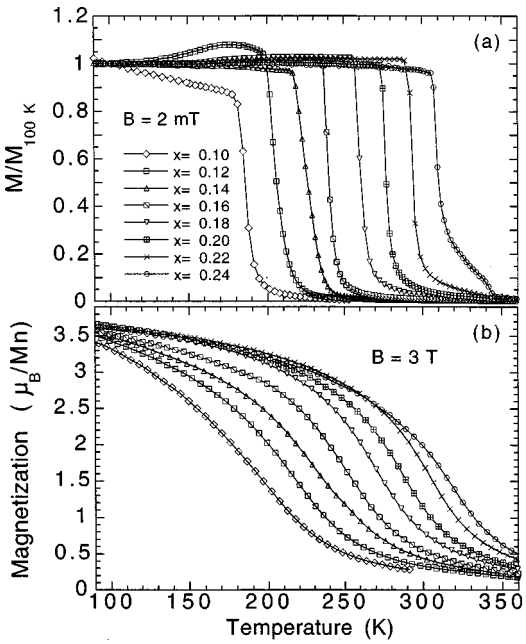

FIG. 5. Magnetization for $La_{1-x}Ba_xMnO_{3.00}$ samples, $x=0.10-0.24$ (in steps of $\Delta x=0.02$) in applied field of 2 mT (a) and 3 T (b).

the existence of a canted ferromagnetic state, similar to that observed for the $La_{1-x}Sr_xMnO_3$ compound with $x=0.125$ (Ref. 18) and for $La_{1-x}Ca_xMnO_3$ with $x\sim0.1-0.2$.[19] A canted ferromagnetic state for our samples with $x=0.10$ and 0.12 is also suggested by the magnetization loops, which begin to saturate only at high magnetic fields, 4 and 2.5 T, respectively. These fields are considerably higher than the saturation fields for magnetization loops obtained for samples with larger Ba contents that begin to saturate at 1.5 T (see Fig. 6). The magnetic transition for the $x=0.24$ sample shows an additional increase of magnetization at $\sim$335 K which probably occurs as a result of the presence of a small fraction of the phase with composition $x\sim0.3$ at the Ba-solubility limit in the perovskite phase. The transition temperatures T_M obtained from the maximum slope of the $M(T)$ curves are listed in Table I. These transition tempera-

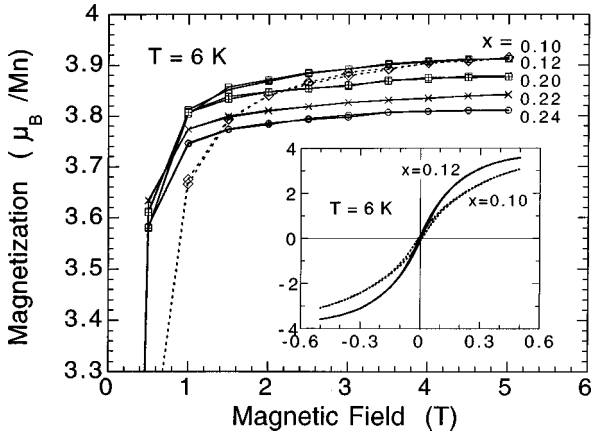

FIG. 6. Magnetization as a function of magnetic field in the vicinity of the saturation values at 6 K for selected samples. Insert: magnetization loops for samples with $x=0.10$ and 0.12.

tures increase almost linearly with the amount of substitution.

Figure 5(b) shows the temperature dependence of the magnetizations for all samples in an applied field of 3 T, i.e., a field high enough to achieve saturation for all samples except for that with $x=0.10$. The $M(T)$ curves show typical features for ferromagnets, i.e., shapes predicted approximately by the mean-field theory and increased transition temperatures in magnetic field. The transitions from the paramagnetic to the ferromagnetic state in high fields correlate very well with the resistivity anomalies for all samples (see Fig. 8 for $x=0.22$).

The ac susceptibility χ_{ac} was measured as a function of temperature for several samples using an ac field with an amplitude of 14 Oe and a frequency of 5 kHz. The data show a pure ferromagnetic order obeying the Curie-Weiss law above the extrapolated transition temperatures T_c equal to 278, 310, and 337 K for samples with $x=0.14$, 0.18, and 0.22, respectively (see Table I). A small ferrimagnetic-like deviation from the linear $1/\chi_{ac}$ vs T dependence was observed for the sample with $x=0.10$, and can be explained as a consequence of the presence of the canted phase, as it was suggested from the dc magnetization experiments. From a fit to the Curie-Weiss law for the data much above T_c, the average effective magnetic moments, μ_{eff}(exp), were calculated and are listed in Table I. These values can be compared with the ideal values $\mu_{eff}(\text{calc})=(1-x)\ \mu_{eff}(Mn^{3+})+x\cdot\mu_{eff}(Mn^{4+})$, by taking $\mu_{eff}(Mn^{3+})=4.90\mu_B$ and $\mu_{eff}(Mn^{4+})=3.87\mu_B$ for the vacancy-free samples with quenched orbital angular momentum ($J=S$) for both Mn ions. The agreement between experimental μ_{eff}(exp) and theoretical μ_{eff}(calc) values is very good (see Table I) and confirms that the spin-orbit coupling for Mn^{3+} and Mn^{4+} is weak in the Ba-substituted material.

Figure 6 shows the magnetization as a function of magnetic field in the vicinity of the saturation values at 6 K for five samples. The $M(H)$ curves for the $x=0.14$, 0.16, and 0.18 samples at fields above 1.5 T lie between the curves for samples with $x=0.12$ and 0.20. The saturation magnetic moments, μ_{sat}(exp), were taken at a field of 6 T as an extrapolated, fully saturated magnetization calculated per Mn ion. These average μ_{sat}(exp) are listed in the Table I for all samples and are compared with the theoretical saturation magnetic moments, $\mu_{sat}(\text{calc})=(1-x)\mu_{sat}(Mn^{3+})+x\mu_{sat}(Mn^{4+})$, where $\mu_{sat}=4\mu_B$ and $3\mu_B$ for Mn^{3+} and Mn^{4+}, respectively. The experimental values for μ_{sat}(exp) (measured with the accuracy of $\pm 0.04\mu_B$) decrease monotonically with the increased hole doping, i.e., with increased Mn^{4+}/Mn^{3+} ratio, and show an excellent agreement with the calculated values μ_{sat}(calc). Because the orbital moment of both Mn ions can be neglected in these compounds, the agreement between measured and calculated saturation magnetic moments suggests that the on-site exchange interaction between itinerant e_g and local t_{2g} electrons is strong enough to align spins completely. The inset to Fig. 6 shows the magnetization loops for samples with $x=0.10$ and 0.12. The loops are broader than for samples with larger Ba contents and saturate at higher fields as observed before. The notable broadening of the magnetization loops, observed in the increased remnant magnetization and compulsion field, and the enhanced saturation fields are consistent with the presence of a canted phase.

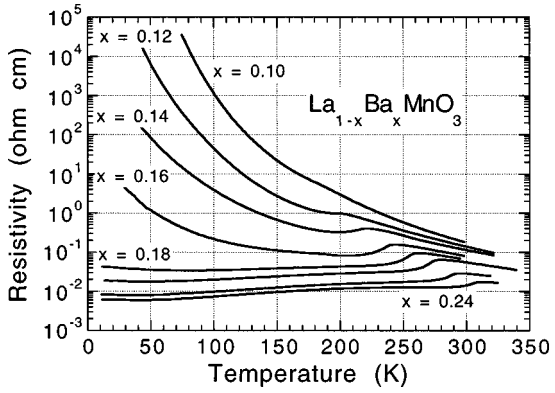

FIG. 7. Resistivity for $La_{1-x}Ba_xMnO_{3.00}$ samples.

Resistivities were measured in the temperature range 6 to 390 K using the standard four-lead dc measurement technique on cut bars with approximate dimensions of $10\times 2\times 1$ mm. The current density used in the measurements was $0.5-50$ mA/cm^2. The resistivities for all samples, shown in Fig. 7, display behavior typical for substituted $LaMnO_3$ samples as a function of the substitution level. With increasing x, samples show a gradual transition from nonmetallic to metallic properties that are marked by a resistive anomaly at temperatures that correlate very well with the magnetic transition temperatures, confirming that the ferromagnetic spin arrangement is a main reason for the colossal magnetoresistance in the vacancy-free compounds. A clear separation of the magnetic transition temperatures from the temperatures of the resistive anomaly were observed for both pure and substituted compounds with large amounts of defects.[20] The temperatures corresponding to the maximum in the $R(T)$ curve, T_R, are listed in Table I. These transition temperatures are slightly higher than for the Sr-substituted samples for small x, $x=0.10-0.14$, and slightly lower for large x, $x=0.20-0.24$.

The dependence of T_c on x is a function of the hole doping and the structural factors that are described in terms of the tolerance factor[9,13,15] and the A-cation size variance.[16] Since the ionic size of Ba is considerably larger than that of Sr, the tolerance factor increases much faster with Ba substitution. This was seen already for the structural properties where the orthorhombic-to-rhombohedral transition appeared near room temperature for $x\sim 0.13$. Also, the magnetoresistive transition temperature for low x appears at higher values because of the better match between the Mn-O and La(Ba)-O bond lengths as described by the tolerance factor or measured by the bond angles. For larger $x\sim 0.2$, the significant La and Ba size difference affects every Mn-O bond, causing local structural distortions as stated by the large value of the A-cation size variance (see Fig. 4). These local structural distortions may be the reason for the lower transition temperatures than for the Sr-substituted samples for $x=0.20-0.24$.

The resistivity at several applied fields (field-cooled sample) is shown in Fig. 8 for the $x=0.22$ substituted sample that has a resistive transition anomaly close to room temperature. The resistive transition temperature gradually increases with increasing applied field at ~ 8 K/T. The magnetoresis-

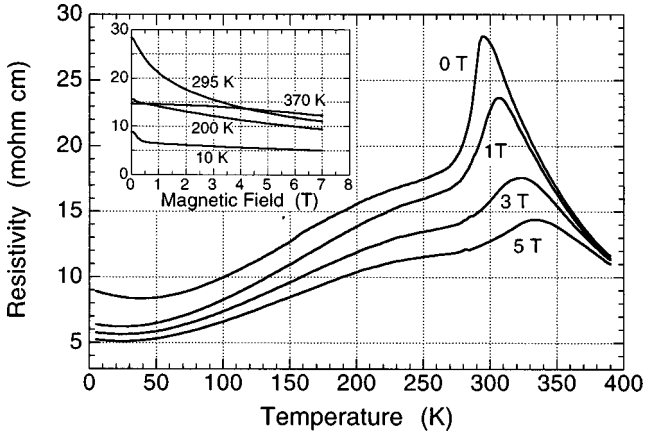

FIG. 8. Resistivity at several applied fields for the $x=0.22$ substituted sample. Insert: resistivity as a function of magnetic field at constant temperatures 370, 295, 200, and 10 K.

tive effect is the largest at 295 K, about -25% at 1 T. A similar result is obtained when resistivity is measured as a function of magnetic field at constant temperature (zero-field-cooled sample) as shown in the inset to Fig. 8. The excellent agreement observed for results obtained for the ''field-cooled'' and ''zero-field-cooled'' measurements is consistent with the absence of a hysteresis effect and reveals that the transport properties are not dependent on the thermal and magnetic history for that composition.

CONCLUSION

Vacancy-free, Ba-substituted, $LaMnO_3$ samples with compositions encompassing structural and magnetoresistive transitions at room temperature have been prepared using thermodynamic information obtained from thermogravimetric analysis measurements. Each composition requires unique synthesis conditions; therefore, using identical conditions for a series of samples will result in materials with varying vacancy content on the metal or oxygen sites. The structural, magnetic, and resistive measurements show that properties are similar to those for the Sr-substituted system but somewhat different from those for Ca-substituted material. Structural properties are governed by the average and variance of the ionic sizes, while resistive and magnetic properties are controlled by both the ionic sizes and the hole doping. The measured and calculated magnetic moments show excellent agreement, confirming that orbital angular momentum is quenched for vacancy-free samples. The optimal composition for applications at room temperature was found at $x=0.22$.

ACKNOWLEDGMENTS

The work at NIU was supported by the ARPA/ONR and at ANL by US DOE (W-31-109-ENG-38).

*Also at Institute of Low Temperature and Structure Research, Polish Academy of Sciences, P.O. Box 937, 50-950 Wroclaw, Poland.

[1] R. von Helmolt, J. Wecker, K. Samwer, L. Haupt, and K. Barner, J. Appl. Phys. **76**, 6925 (1994).
[2] J. A. M. Van Roosmalen, E. H. P. Cordfunke, and R. B. Helmholdt, and H. W. Zandbergen, J. Solid State Chem. **110**, 100 (1994).
[3] J. Toepfer and J. B. Goodenough, Chem. Mater. **9**, 1467 (1997).
[4] J. A. M. Van Roosmalen and E. H. P. Cordfunke, J. Solid State Chem. **110**, 106 (1994).
[5] M. Hervieu, R. Mahesh, N. Rangavittal, and C. N. R. Rao, Eur. J. Solid State Inorg. Chem. **32**, 79 (1995).
[6] H. L. Ju, J. Gopalakrishnan, J. L. Peng, Qi Li, G. C. Xiong, T. Venkatesan, and R. L. Greene, Phys. Rev. B **51**, 6143 (1995).
[7] A. Urushibara, Y. Moritomo, T. Arima, A. Asamitsu, G. Kido, and Y. Tokura, Phys. Rev. B **51**, 14 103 (1995).
[8] A. Asamitsu, Y. Moritomo, Y. Tomioka, T. Arima, and Y. Tokura, Nature (London) **373**, 407 (1995).
[9] H. Y. Hwang, S-W. Cheong, P. G. Radaelli, M. Marezio, and B. Batlogg, Phys. Rev. Lett. **75**, 914 (1995).
[10] J. F. Mitchell, D. N. Argyriou, C. D. Potter, D. G. Hinks, J. D. Jorgensen, and S. D. Bader, Phys. Rev. B **54**, 6172 (1996).
[11] Mitsuru Itoh, Kojiro Nishi, Jian Ding Yu, and Yoshiyuki Inaguma, Phys. Rev. B **55**, 14 408 (1997).
[12] A. C. Larson and R. B. Von Dreele, General Structure Analysis System University of California, Berkeley, 1985–1990.
[13] R. D. Shannon, Acta Crystallogr., Sect. A: Cryst. Phys., Diffr., Theor. Gen. Crystallogr. **32**, 751 (1976).
[14] B. Dabrowski (unpublished).
[15] W. Archibald, J.-S. Zhou, and J. B. Goodenough, Phys. Rev. B **53**, 14 445 (1996).
[16] L. M. Rodriguez-Martinez, and J. P. Attfield, Phys. Rev. B **54**, R15 622 (1996).
[17] P. Schiffer, A. P. Ramirez, W. Bao, and S.-W. Cheong, Phys. Rev. Lett. **75**, 3336 (1995).
[18] D. N. Argyriou, J. F. Mitchell, C. D. Potter, D. G. Hinks, J. D. Jorgensen, and S. D. Bader, Phys. Rev. Lett. **76**, 3826 (1996).
[19] G. Matsumoto, J. Phys. Soc. Jpn **29**, 615 (1970).
[20] S. Yang, C. T. Lin, K. Rogacki, B. Dabrowski, P. M. Adams, and D. M. Speckman, Chem. Mater. **10**, 1374 (1998).